Han *et al. Int J Concr Struct Mater (2018) 12:53*
https://doi.org/10.1186/s40069-018-0268-1

International Journal of Concrete Structures and Materials

ORIGINAL ARTICLE

Open Access

Flexural Responses of Prestressed Hybrid Wide Flange Composite Girders

Sun-Jin Han[1], Deuck Hang Lee[2], Jae-Yuel Oh[3], Seung-Ho Choi[1] and Kang Su Kim[1*]

Abstract

In this study, prestressed hybrid wide flange (PHWF) composite girders were proposed, and full-scale flexural tests were conducted to evaluate their structural performances. This new proposed girder system was developed and designed to effectively resist external loads considering the actual construction sequences. Two specimens with and without shear connectors were fabricated and tested to examine the effect of the shear connectors for achieving the fully-composite behaviors between a cast-in-place (CIP) concrete and the prefabricated prestressed steel–concrete composite girder. The test results showed that sufficient flexural strengths and deformation capacities can be obtained in both types of PHWF composite girders with and without shear connectors. To reflect the actual construction stages of the proposed PHWF composite girder, nonlinear flexural analyses were proposed considering the prestress effect and segmental effect before and after composite with the CIP concrete, respectively. The observed and analysis results of strain behaviors of the PHWF girder specimens were also compared and discussed in detail.

Keywords: hybrid beam, composite member, prestressed concrete, wide flange, non-linear analysis

1 Introduction

Steel–concrete composite members have been widely used in constructions of buildings and civil engineering structures because of their excellent structural performances based on the efficient use of steel and concrete materials. In particular, as contemporary structures are being constructed higher and larger due to the development of high strength materials with the continued advances in construction technologies, various composite structural systems have been developed and proposed that can realize the long-span structures and reduce floor heights (Ayyub et al. 1990, 1992a, b; Kim et al. 2002, 2009). Figure 1 shows various composite structural members developed from previous researches (Azizinamini et al. 2004; Bae and Lee 2007; Abbas et al. 2007; Heo et al. 2007; Hong et al. 2010a, b, c, d; Kim et al. 2011, 2013; Kim and Lee 2011; Oh et al. 2012, 2015; Lee et al. 2015), among which the prestressed composite systems can lead to enhance the strength, ductility, and serviceability of the structural members, utilizing the prestressing force introduced to the concrete. Although many other steel–concrete composite girder systems have been developed, as shown in Fig. 1, increasing demand continues for new horizontal composite members that can ensure reliable load-carrying performances and price competitiveness in the current construction market (Heo et al. 2007; Kim et al. 2011; Kim and Lee 2011). Therefore, in this study, the prestressed hybrid wide flange (PHWF) girder that can effectively resist external forces was developed. Figure 2 shows the main concepts and the actual construction sequences of the proposed PHWF girder. The PHWF girder system was devised and designed to achieve superior deflection control performance and high flexural and shear capacities by introducing prestress into the concrete bottom flange. In addition, by utilizing the embedded steel member with trapezoidal-shaped multiple openings (Fig. 2), the horizontal shear strength and the composite performance between the cast-in-place (CIP) concrete and the PHWF girder can be significantly enhanced. In addition, the top steel flange of the embedded steel member was designed to achieve the sufficient capacity under positive flexural moments

*Correspondence: kangkim@uos.ac.kr
[1] Department of Architectural Engineering, University of Seoul, 163 Siripdaero, Dongdaemun-gu, Seoul 02504, South Korea
Full list of author information is available at the end of the article
Journal information: ISSN 1976-0485 / eISSN 2234-1315

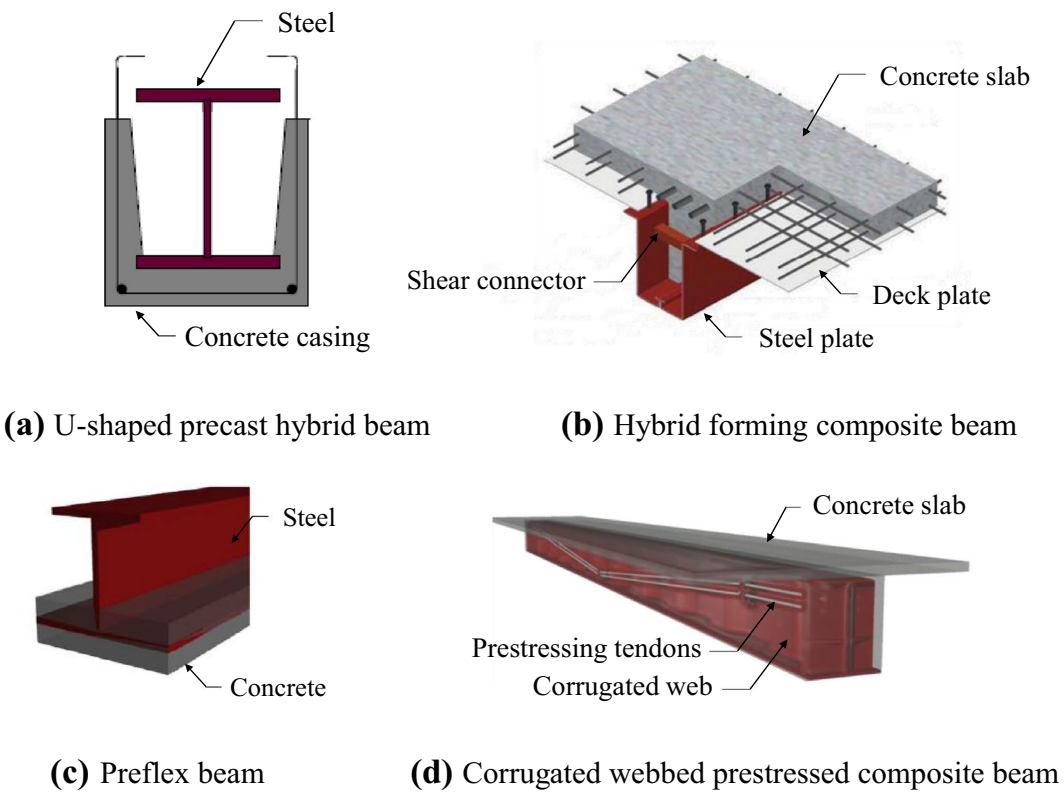

Fig. 1 Various composite structural members in literature.

induced by construction loads before composite with the CIP topping concrete. As shown in the central part of Fig. 2, the width of the prestressed concrete (PSC) bottom flange was intentionally designed to be large, so that deep steel deck plates can be placed on the PSC bottom flange, and the reinforcing bars placed in the slab can be easily passed through the trapezoidal-shaped openings in the embedded steel member for continuous connections, as depicted on the right hand side of Fig. 2. In this study, flexural tests on the PHWF composite girders were conducted to investigate their flexural performances, and the test results are discussed in detail. In addition, a nonlinear flexural analysis model was proposed considering the unique strain distributions of the PHWF composite girder before and after the integration with the CIP concrete due to the prestress segmental effect. The analysis results were then compared with the experimental results for verification.

2 Experimental Program

2.1 Test Specimens

As shown in Fig. 3 and Table 1, two composite girder specimens, named as US-F1 and US-F2, were fabricated and tested in this study. Shear studs were placed at 100 mm spacing on the top flange of the embedded steel member for the US-F1 specimen, while shear studs were not used in the US-F2 specimen. But instead, for the US-F2 specimen, the top flange of the embedded steel member was extended to the mid-depth of the CIP concrete slab to enhance the horizontal shear capacity as shown in Fig. 3b. The heights (h) of the US-F1 and US-F2 specimens before composite with the CIP concrete (i.e. prefabricated steel member embedded in PSC bottom flange) were 530 and 585 mm, respectively. The embedded steel member, shown at the top of Fig. 2, was fabricated using Grade SS400 steel material with 6 mm thick plates, and its yield and tensile strengths (F_y and F_u) were 281.7 and 436.7 MPa, respectively. As shown in Fig. 3, the top flange of the embedded steel member was additionally reinforced using a 40 mm × 40 mm rectangular solid steel bar to provide sufficient resistance to the compressive stress induced by the construction loads. At the actual construction site, the PHWF composite girder system is integrated with the CIP concrete by installing deep steel deck plates on the PSC bottom flange. However, the slab deck plate was not used in the test specimens for better crack observations and recordings during testing. As shown in Table 1, the compressive

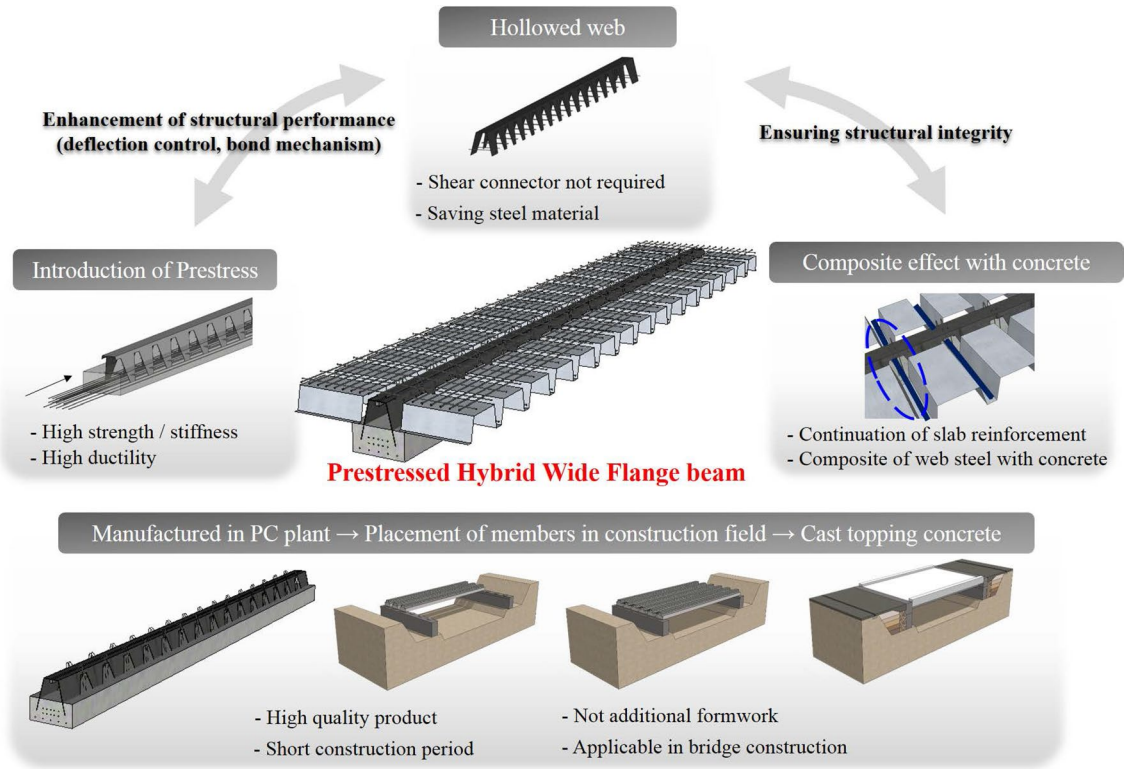

Fig. 2 Concept of PHWF composite girder.

strengths of concrete used in the PSC bottom flange and the CIP concrete were 35.2 and 30.0 MPa, respectively, and the concrete strains corresponding to the compressive strengths (ε_c') were 0.0025 and 0.0023, respectively. In the PSC bottom flange, ten low-relaxation seven-wire strands of Grade 1860 MPa and five M16 reinforcing bars of Grade 420 MPa were provided in the longitudinal direction. The average yield strength of the reinforcing bars (f_y) was 466.3 MPa, and the average yield and tensile strengths of the prestressing strands (f_{py} and f_{pu}) were 1815.0 and 1928.7 MPa, respectively. Figure 4a shows the fabrication process of the test specimens. The prestressing strands were tensioned using a hydraulic jack and anchored to the buttresses of the prestressing bed after the formworks for the PSC bottom flange. Two M10 shear reinforcements with 501.7 MPa yield strength were placed within each opening through the shear spans of the test specimens. Then embedded steel member with trapezoidal-shaped multiple openings was placed and, as shown in Fig. 4b, the concrete was cast only in the PSC bottom flange. The load cell was installed in front of a hydraulic jack to precisely control the jacking stress (f_{pj}) up to the target prestress level of $0.7f_{pu}$. The specimens then underwent steam curing for 2 days, and the prestresses were released when the compressive strength of the immature concrete (f_{ci}) reached 20.7 MPa. The measured effective prestress (f_{pe}) at prestress transfer was $0.61f_{pu}$. As shown in Fig. 4c, d, M10 compressive reinforcements were placed in the CIP concrete slab after installation of the slab formwork. The CIP concrete was then cast and cured for 28 days.

2.2 Measurements and Test Apparatus

Figure 5 shows the details of strain gages and linear variable differential transformers (LVDTs) installed to measure the deformation behaviors of the test specimens. To measure the strain distribution in the cross-section, the seven strain gages were attached to the constant flexural moment region in the vertical direction. Three and two concrete strain gages were attached to the upper and lower surfaces, respectively, of the CIP concrete slab at 300 mm spacing to investigate the strain behaviors of the compression zone. LVDTs were also installed to measure the vertical deflection of the test specimens and end slips between the PSC bottom flange and CIP concrete member. Figure 6 shows the test set-up of the specimens immediately before load applications; Two-point loads were applied with a loading rate of 0.015 mm/sec using a 1000 kN capacity actuator, which was controlled by the displacement. The distance between supports was

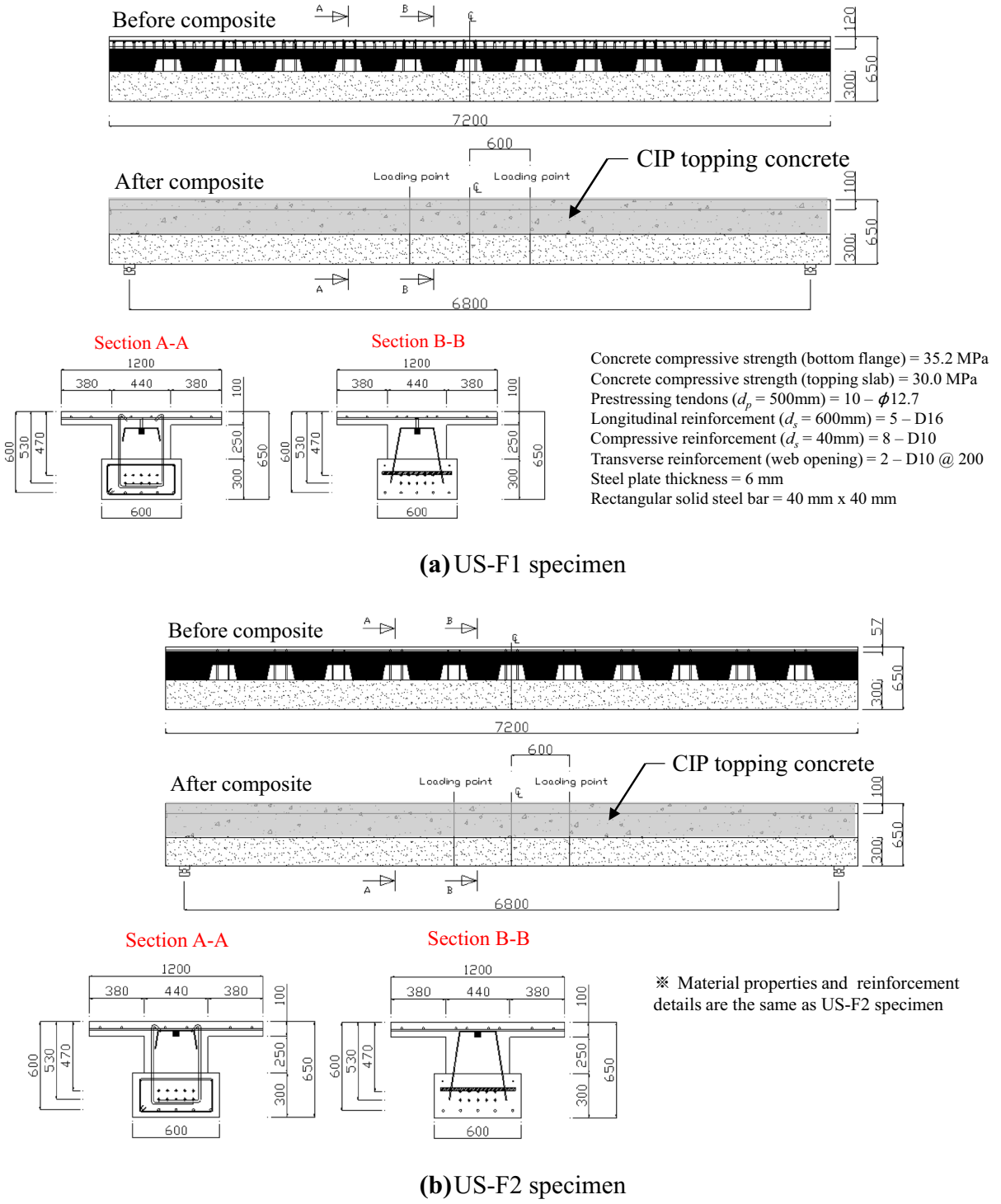

Fig. 3 Dimensional details of test specimens (unit: mm).

6800 mm, the distance from the support to the loading point was 2800 mm, and the distance from the loading point to the center of the specimen was 600 mm.

2.3 Flexural Responses Measured from Experiments

Figure 7 shows the crack patterns at failures of the specimens. The two specimens showed typical

Table 1 Dimensional details of test specimens.

Steel plate (SS400)		Steel reinforcement				Tendon		Concrete	
6 mm		10 mm		16 mm				Bottom flange	Topping concrete
F_y (MPa)	F_u (MPa)	f_y (MPa)	f_u (MPa)	f_y (MPa)	f_u (MPa)	f_{py} (MPa)	f_{pu} (MPa)	f_{ck} (MPa)	
281.7	436.7	501.7	618.9	466.3	604.7	1815.0	1928.7	35.2	30.3

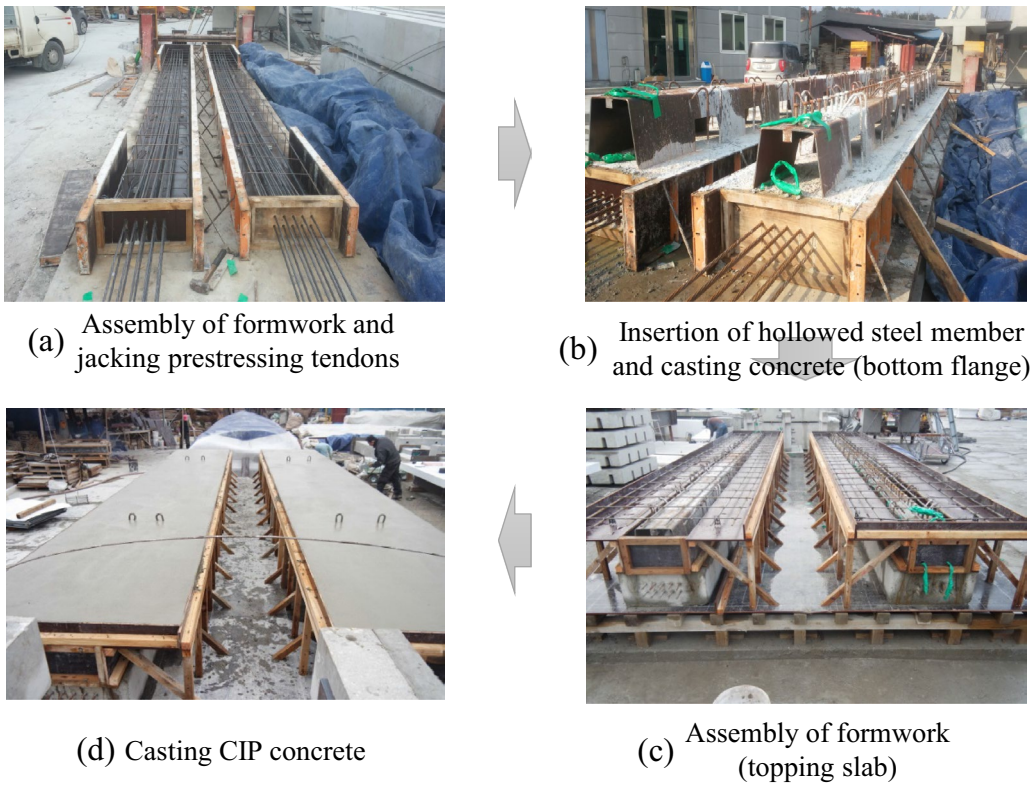

Fig. 4 Fabrication process of test specimens.

flexural-dominant behaviors and crushing failure mode at the extreme compression fiber of the composite section with sufficient ductility. Figure 8 shows the flexural responses of the test specimens, and the major events of which are marked. In the US-F1 specimen, the initial flexural cracks were observed at 248 kN of the load (central deflection of 4 mm), and the inclined shear cracks occurred at 529 kN (central deflection of 17 mm). At a load of 710 kN (central deflection of 33 mm), the flexural stiffness was significantly reduced due to yielding of the flexural tension reinforcements. Subsequently, the stress in the prestressing strands significantly increased, and the specimen finally failed with the concrete crushing at the compression zone of the constant moment region at a load of 922 kN (central deflection of 119 mm). Even though the US-F2 specimen contained no shear connectors, it showed a ductile flexural behavior very similar to that of the US-F1 specimen. Flexural cracks occurred at a load of 260 kN (central deflection of 4 mm), and the tensile reinforcements yielded at a load of 672 kN (central deflection of 29 mm). Finally, the specimen showed concrete crushing on the compressive zone near the loading point at a load of about 917 kN (central deflection of 109 mm). The two specimens showed similar flexural strengths and deformational capacities, indicating that the fully-composite actions between the PHWF composite girder and the CIP concrete can be sufficiently achieved by extending the height of the top flange of the embedded steel member within the CIP slab member, instead of using shear studs.

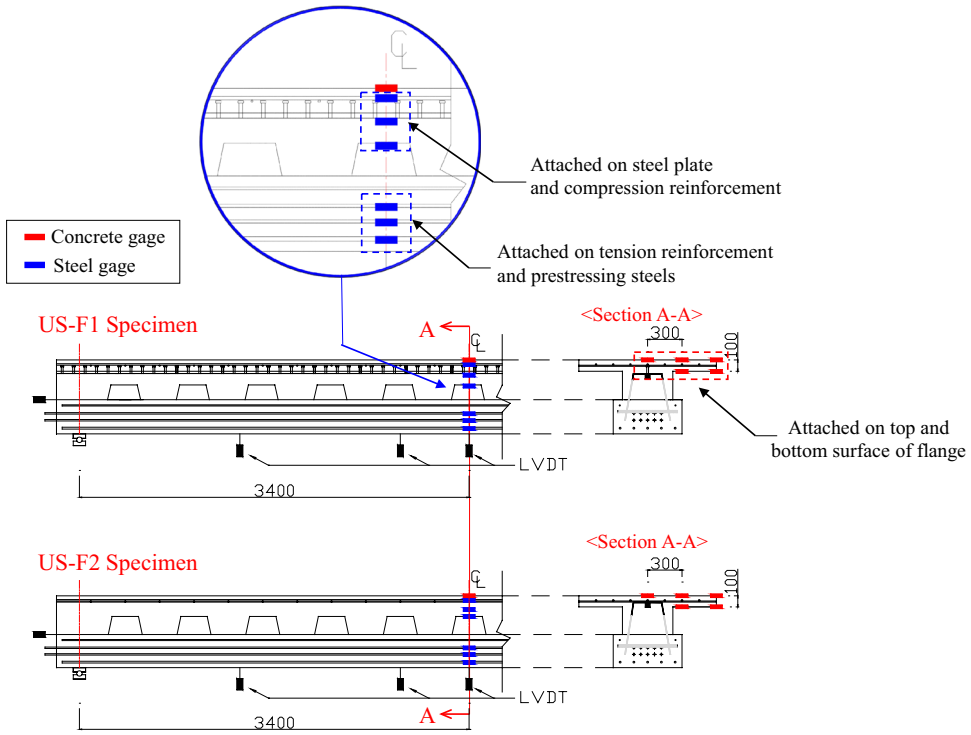

Fig. 5 Details of strain gages and measuring devices (unit: mm).

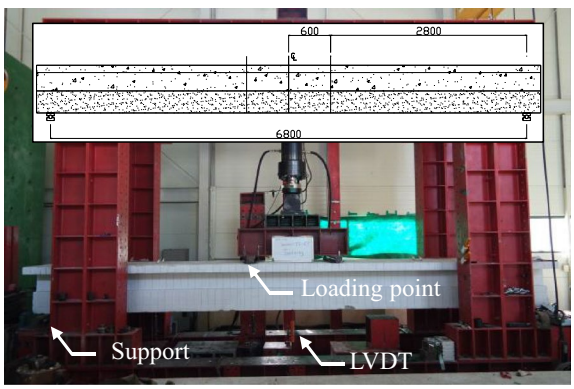

Fig. 6 Test set-up.

2.4 Measured Strain Distributions and End Slip

Figure 9 shows the strain behaviors of the test specimens measured from the concrete gages attached to the upper and lower surfaces of the CIP concrete slab. As shown in Fig. 9a, the US-F1 specimen showed almost the same and continuously increasing responses for the normal strains measured from the top surfaces of the CIP concrete slab (gage Nos. ①, ②, and ③). On the other hand, the compressive strains measured from the bottom surface of the CIP concrete slab (gage Nos. ④ and ⑤) showed an increasing tendency up to a load of 650 kN. The compressive strains then decreased but remained in compression, at which the neutral axis appeared to be located within the CIP concrete slab. In the case of the US-F2 specimen shown in Fig. 9b, the concrete strains measured from the bottom surfaces of the CIP concrete slab (gage Nos. ④ and ⑤) significantly changed from compression to tension and reached a very large tensile strain; the direction of the strain behaviors then changed at the higher load level compared to that of the US-F1 specimen. This is because the top flange of the embedded steel member of the US-F2 specimen was placed deep inside the CIP concrete slab; the neutral axis of the US-F2 specimen was, therefore, located at a considerably higher position within the CIP concrete slab at failure compared to that of the US-F1 specimen.

Figure 10 shows the strain distributions of the US-F1 and US-F2 specimens along the member height direction according to different loading stages. The strains measured in the direction of the member height quite clearly showed linear stain distributions up to the maximum load. As shown in Fig. 11, the end slip between the PSC bottom flange and the CIP concrete rarely occurred for all specimens, indicating that the PSC bottom flange, the embedded steel member, and the CIP concrete

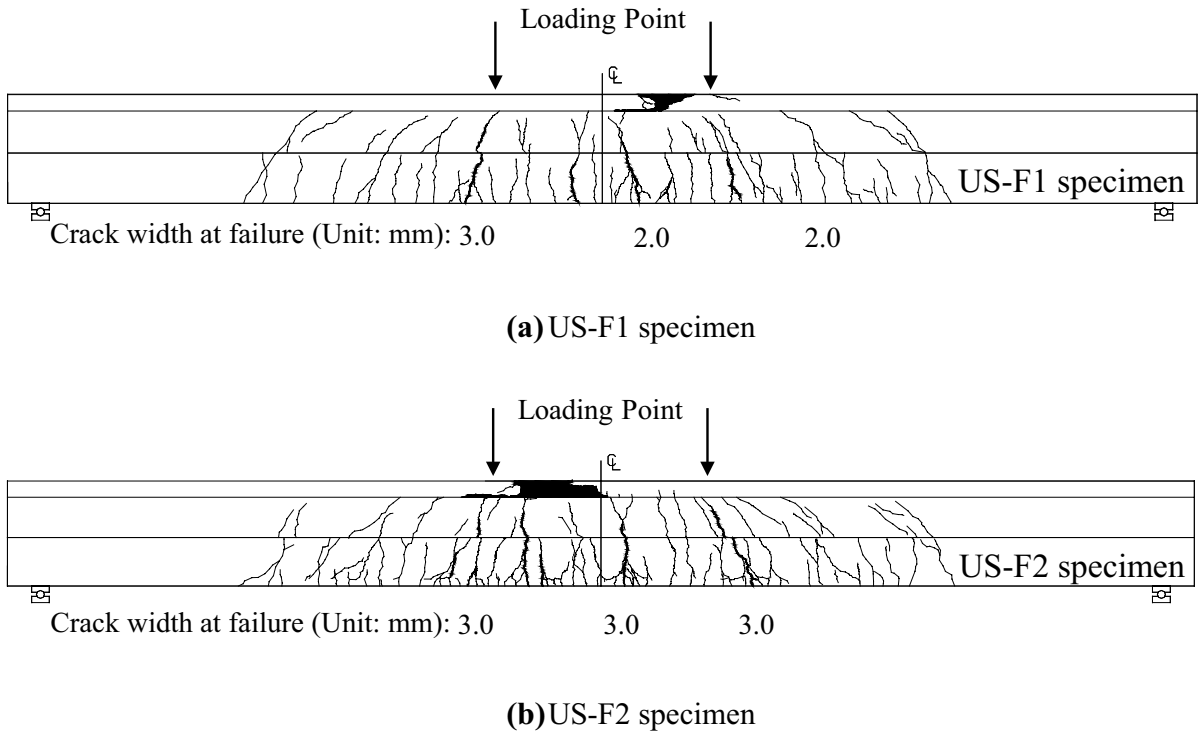

Fig. 7 Crack patterns of test specimens at failure.

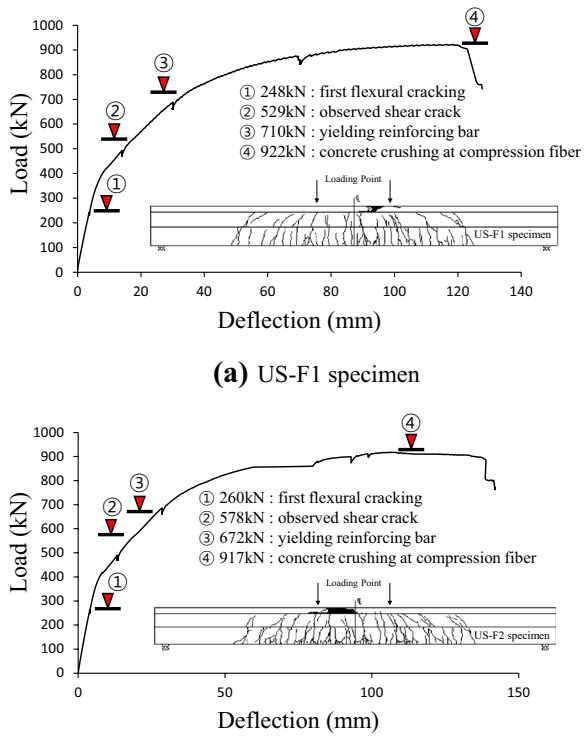

Fig. 8 Load-deflection response curves of test specimens.

showed almost fully-composite behaviors. The end slips observed in the US-F1 specimen at the maximum load was 0.136 mm, which is slightly larger than 0.015 mm of the US-F2 specimen. Assuming that the strain differences between the PSC bottom flange and the CIP concrete are uniformly distributed in the longitudinal direction from the support to the loading point, the average strain difference between the PSC bottom flange and the CIP concrete ($\varepsilon_{topping} - \varepsilon_{bottom}$) can be calculated, as follows:

$$\varepsilon_{topping} - \varepsilon_{bottom} = \frac{s}{a} \tag{1}$$

where $\varepsilon_{topping}$ and ε_{bottom} are the strains of the CIP concrete and the PSC bottom flange, respectively, at their interface, s is the measured end slip (mm), and a is the length of shear-span (mm). The average strain difference of the US-F1 and US-F2 specimens calculated from Eq. (1) was 4.8×10^{-5} and 5.3×10^{-6}, respectively, and thus the strain difference between the PSC bottom flange and the CIP topping concrete were small enough to be ignored. On this basis, a linear strain distribution within the cross section (i.e. Bernoulli's plane section remaining plane hypothesis) can be assumed in the nonlinear flexural analysis of the PHWF composite girder, as explained in the following section.

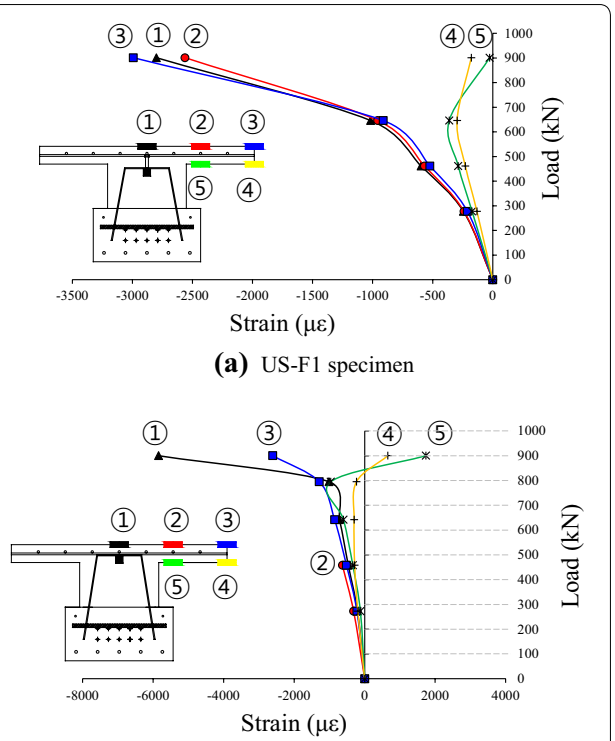

(a) US-F1 specimen

(b) US-F2 specimen

Fig. 9 Measured strain distributions at CIP concrete slabs.

3 Comparison of Nonlinear Flexural Behavior Model and Experimental Results

3.1 Nonlinear Flexural Behavior Model for PWHF Girder

Figure 12a shows the strain distribution induced by the introduction of the prestress to the PWHF girder before composite with the CIP concrete. Here ε_{pe} is the effective prestrain of prestressing strands, $\varepsilon_{sf,b}$, $\varepsilon_{psp,b}$, $\varepsilon_{s,b}$, and $\varepsilon_{ps,b}$ are the prestrains of the compressive flange of the embedded steel member, the rectangular solid steel bar, the reinforcing bars, and the prestressing strands, respectively, $C_{c,b}$ and $C_{s,b}$ are the compression force of concrete and steel reinforcement after prestress release (N), respectively, T_{pe} is the effective prestressing force (N), and $T_{sf,b}$, $T_{w,b}$ and $T_{sp,b}$ are the force of embedded steel flange, web, and solid steel bar after prestress release (N), respectively. As shown in Fig. 12, if the section is divided into i number of layers in the transverse direction, the longitudinal strain ($\varepsilon_{i,pre}$) at the ith layer immediately after the prestress release can be calculated, as follows:

$$\varepsilon_{i,pre} = -\frac{P_e}{E_{ci}A_t} \pm \frac{P_e e_p}{E_{ci}I_b} y_i \mp \frac{M_d}{E_{ci}I_b} y_i \tag{2}$$

where P_e is the effective prestressing force (N), e_p is the eccentricity of prestressing tendons (mm), A_t is the transformed sectional area (mm^2), I_b is the moment of inertia of the section about the centroidal axis (mm^4), M_d is the bending moment induced by the self-weight of the girder (N mm), y_i is the distance from the centroid of the section to the ith layer (mm), E_{ci} is the modulus of elasticity of concrete at the prestress transfer, which was taken to be $4700\sqrt{f_{ci}}$ as presented in ACI318-14 (2014), and f_{ci} is the compressive strength of concrete at prestress transfer. Figure 12b, c show the strain and stress distributions and corresponding sectional forces of the PWHF girder after composite with the CIP concrete at the linear-elastic stage and non-linear stage, respectively. If the concrete strain at the extreme compression fiber (ε_t) is selected, and the concrete strain at the extreme tension fiber (ε_b) is assumed to be an arbitrary value, the strain terms of all the components including the compression flange of the embedded steel member (ε_{sf}), the rectangular solid steel bar (ε_{sp}), the reinforcing bars (ε_s), and the prestressing strands (ε_{ps}) can be calculated considering the effect of the prestrains ($\varepsilon_{sf,b}$, $\varepsilon_{sp,b}$, $\varepsilon_{s,b}$, and $\varepsilon_{ps,b}$, respectively) induced in the section before composite with the CIP concrete shown in Fig. 12a, as follows:

$$\varepsilon_{sf} = \varepsilon_t + \frac{\varepsilon_b - \varepsilon_t}{h} d_{f1} + \varepsilon_{sf,b} \tag{3a}$$

$$\varepsilon_{sp} = \varepsilon_t + \frac{\varepsilon_b - \varepsilon_t}{h} d_{f2} + \varepsilon_{sp,b} \tag{3b}$$

$$\varepsilon_s = \varepsilon_t + \frac{\varepsilon_b - \varepsilon_t}{h} d_s + \varepsilon_{s,b} \tag{3c}$$

$$\varepsilon_{ps} = \varepsilon_{pi} + \frac{\varepsilon_b - \varepsilon_t}{h} d_p + \varepsilon_{ps,b} \tag{3d}$$

where h is the member height (mm), d_{f1}, d_{f2}, d_s, and d_p are the depth of the compressive flange of the embedded steel member, the rectangular solid steel bar, the tensile reinforcement and the prestressing strands (mm), respectively, and ε_{pi} is the initial prestrain in prestressing strands. The strain of the compression reinforcement in the CIP concrete slab (ε'_s) can be calculated, as follows:

$$\varepsilon'_s = \varepsilon_t + \frac{\varepsilon_b - \varepsilon_t}{h} d_{cs} \tag{4}$$

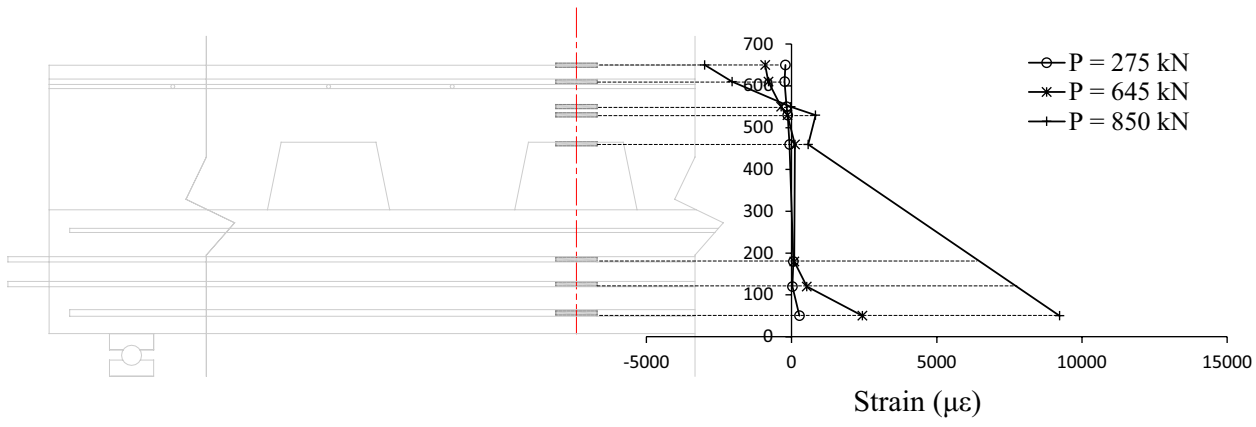

(a) US-F1 specimen

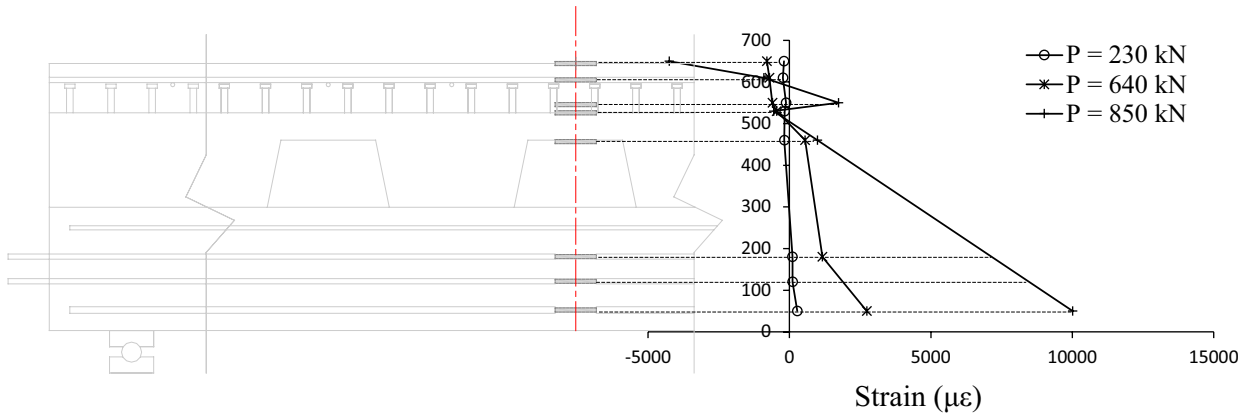

(b) US-F2 specimen

Fig. 10 Measured strain distributions along the member height depending on loading stages.

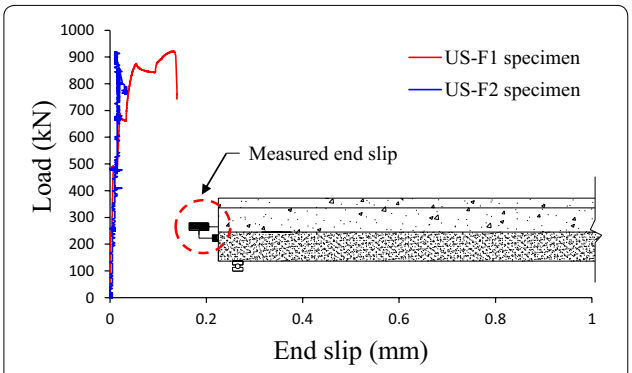

Fig. 11 Measured end slip behaviors between prestressed concrete bottom flange and surrounding CIP concrete.

where d_{cs} is the depth of the compression reinforcement (mm). The stresses corresponding to each strain can be determined by substituting the strains of the steel plate, the steel reinforcement and the prestressing strands obtained from Eq. (3) with the constitutive models of the materials. As shown in Fig. 13a, b, the constitutive equations of the prestressing strands, the steel reinforcement, and the steel plate used in this study can be expressed, as follows (Collins and Mitchell 1991):

$$f_{ps} = E_p \varepsilon_{ps} \left\{ 0.025 + \frac{0.975}{\left[1 + \left(118\varepsilon_{ps}\right)^{10}\right]^{0.1}} \right\} \leq f_{pu} \tag{5}$$

$$f_s = E_s \varepsilon_{sr} \leq f_y \tag{6a}$$

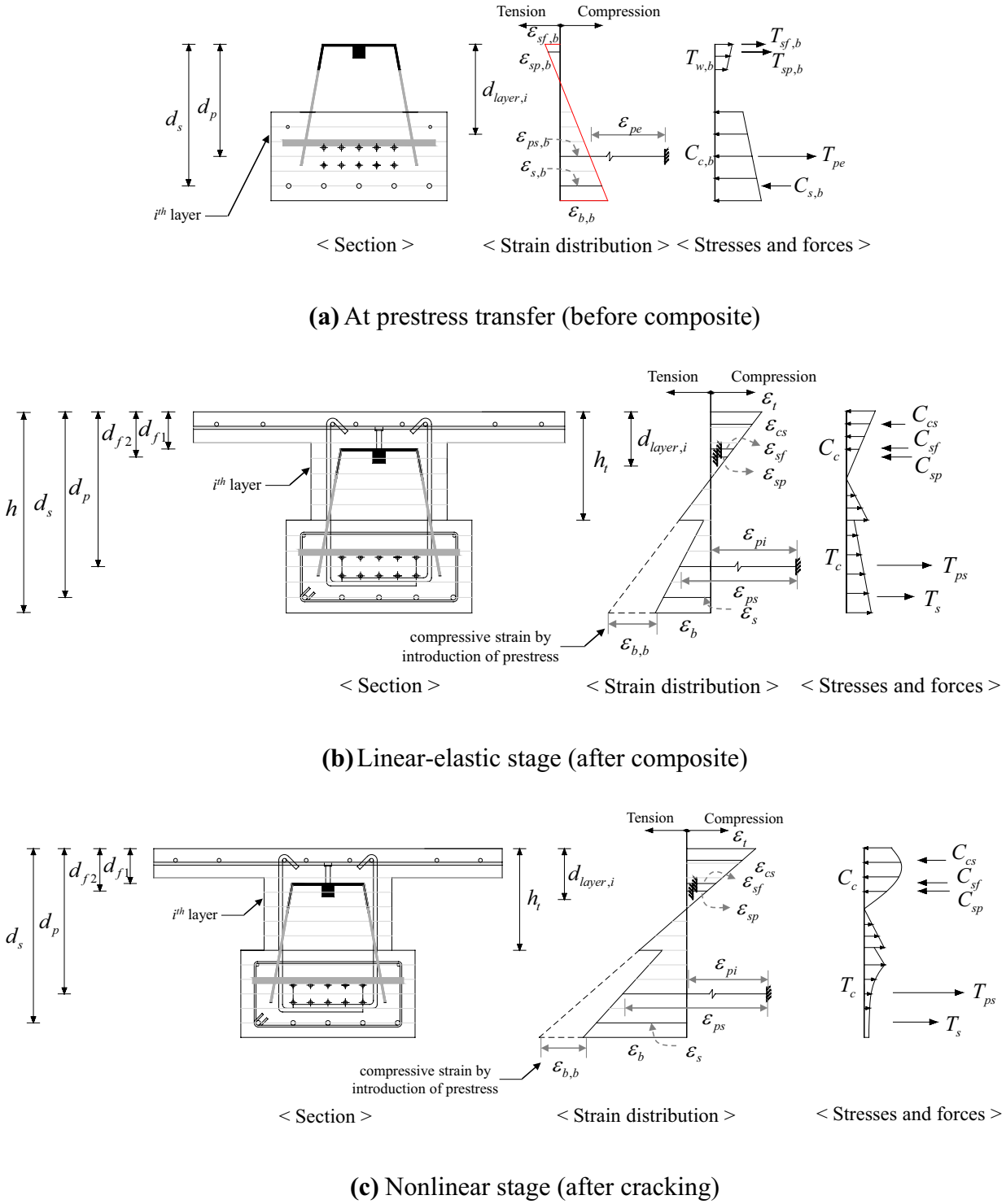

Fig. 12 Proposed sectional analysis model for PHWF girder.

$$F_s = E_s \varepsilon_{ss} \leq F_y \tag{6b}$$

where f_{ps}, f_s and F_s are the stresses of the prestressing strands, the reinforcing bar and the steel plate, respectively (MPa), E_s and E_p are the modulus of elasticity of the reinforcing bar and the prestressing steel, respectively (MPa), ε_{sr} and ε_{ss} are the strains of the reinforcing bar and the steel plate, respectively, and f_y and F_y

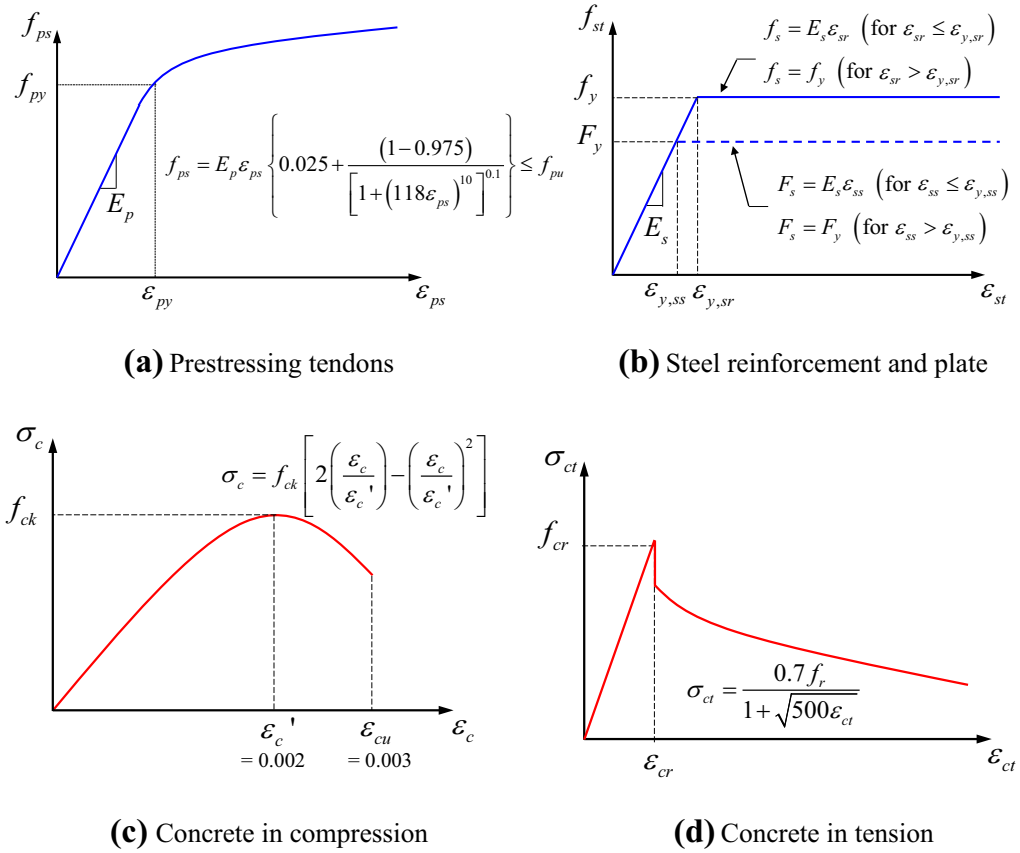

Fig. 13 Constitutive models of materials used in flexural analysis.

are the yield strength of the reinforcing bar and the steel plate, respectively (MPa). The CIP concrete part experiences no initial prestrain, but the PSC bottom flange and the embedded steel member undergo prestrain before composite with the CIP concrete. Therefore, the concrete strain of the PSC bottom flange and the embedded steel member should be estimated considering the precompressive strain as shown in Fig. 12b, c, respectively. Accordingly, the concrete strains of the CIP concrete and the PSC bottom flange at the *i*th layer ($\varepsilon_{c,i}$) can be calculated, respectively, as follows:

$$\varepsilon_{c,i} = \varepsilon_t + \frac{\varepsilon_b - \varepsilon_t}{h} d_{layer,i} \quad (\text{for } 0 \le d_{layer,i} < h_t). \tag{7a}$$

$$\varepsilon_{c,i} = \varepsilon_t + \frac{\varepsilon_b - \varepsilon_t}{h} d_{layer,i} + \varepsilon_{i,pre} \quad (\text{for } h_t \le d_{layer,i} < h) \tag{7b}$$

where h_t is the height from the top of bottom flange to the extreme compression fiber of PHWF girder (mm), and $d_{layer,i}$ is the effective depth of *i*th layer (mm). As shown in Fig. 13c, d, if the concrete strains are obtained from Eq. (7), the corresponding compressive and tensile stresses of concrete at the *i*th layer ($\sigma_{c,i}$ and $\sigma_{ct,i}$) can be estimated using the constitutive equations (Collins and Mitchell 1991), as follows:

$$\sigma_{c,i} = f_{ck}\left[2\left(\frac{\varepsilon_{c,i}}{\varepsilon_c'}\right) - \left(\frac{\varepsilon_{c,i}}{\varepsilon_c'}\right)^2\right] \quad (\text{for } \varepsilon_{c,i} \le 0) \tag{8a}$$

$$\sigma_{ct,i} = E_c\varepsilon_{c,i} \quad (\text{for } 0 < \varepsilon_{c,i} \le \varepsilon_{cr}) \tag{8b}$$

$$\sigma_{ct,i} = \frac{0.7f_r}{1+\sqrt{500\varepsilon_{c,i}}} \quad (\text{for } \varepsilon_{c,i} > \varepsilon_{cr}) \tag{8c}$$

where E_c is the modulus of the elasticity of the concrete (MPa), ε_{cr} is the cracking strain corresponding to f_r, and f_r is the modulus of rupture, which was taken as $0.62\sqrt{f_{ck}}$ (ACI committee 318 2014). After the stresses at each concrete layer are determined, the compressive

force (C_c) and tensile force (T_c) of concrete can be calculated, as follows:

$$C_c = \sum_{\varepsilon_{c,i} \le 0} \sigma_{c,i} b d_y \tag{9a}$$

$$T_c = \sum_{\varepsilon_{c,i} > 0} \sigma_{ct,i} b d_y \tag{9b}$$

where b is the beam width (mm) and d_y is the thickness of the ith layer (mm). As shown in Fig. 12, the normal forces of the compressive flange of the embedded steel member (C_{sf}), the rectangular solid steel bar (C_{sp}), the tension reinforcements (T_s), the compression reinforcements (C_{cs}), and the prestressing strands (T_{ps}) can be calculated by multiplying the stresses obtained from Eqs. (3)–(6) by each cross-sectional area, and the sum of these normal forces should satisfy the equilibrium condition, as follows:

$$C_c + C_{cs} + C_{sf} + C_{sp} + T_c + T_s + T_{ps} = 0 \tag{10}$$

If the equilibrium condition is satisfied, the flexural moment (M) and the curvature (ϕ) can be estimated, respectively, as follows:

$$M = \sum_{d_{layer,i} \le c} C_i d_{layer,i} + \sum_{d_{layer,i} > c} T_i d_{layer,i} \tag{11}$$

$$\phi = \frac{\varepsilon_t}{c} \tag{12}$$

where c is the neutral axis depth. Figure 14 shows the flexural moment and curvature diagrams in the longitudinal direction of the PHWF composite girder subjected to 2-point loading. The relative displacement ($\delta_{j+1,j}$) between the jth and $j+1$th segments can be calculated from the first moment of area on the curvature diagram (Collins and Mitchell 1991), as follows:

$$\delta_{j+1,j} = \int_{x_j}^{x_{j+1}} \phi\left(x_{j+1} - x\right) dx \tag{13}$$

On this basis, the vertical deflection at the center of the member (Δ) can also be calculated, as follows.

$$\Delta = \int_0^{0.5l} \phi x dx \tag{14}$$

where l is the span length of the member. However, since it is difficult to directly solve the integral equation shown

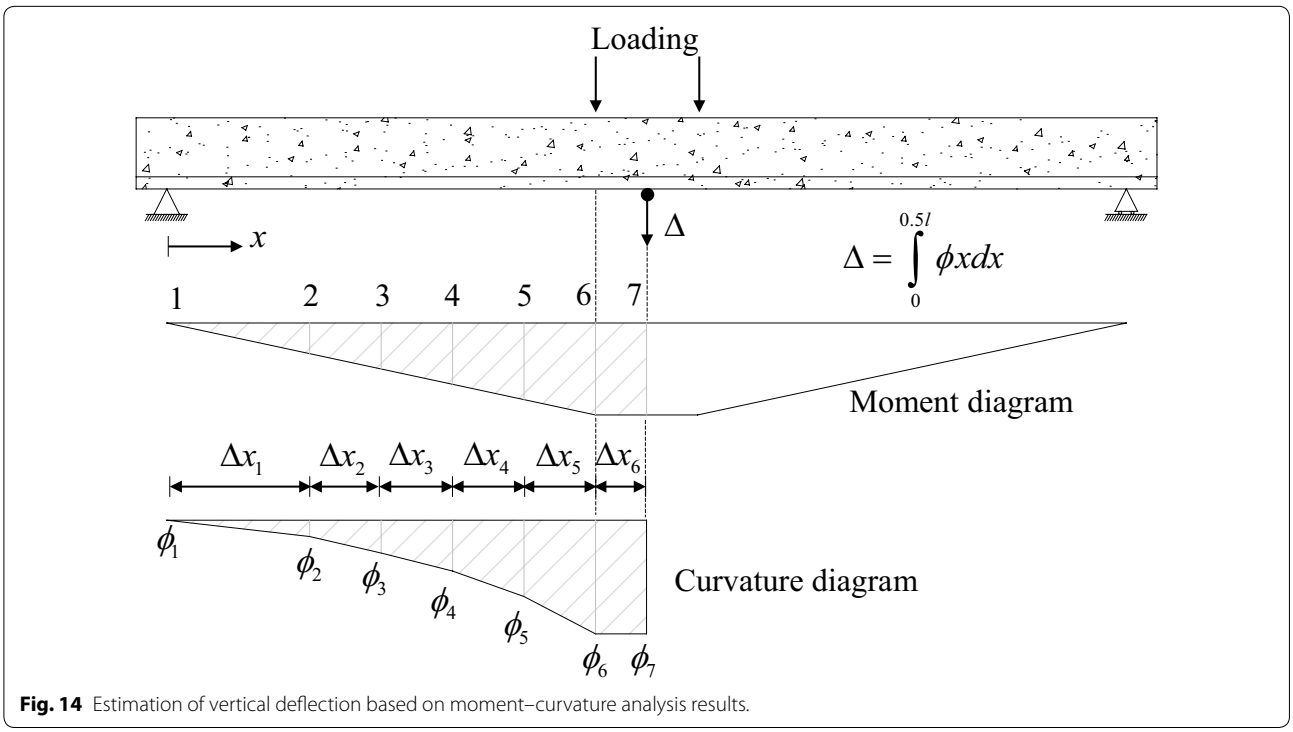

Fig. 14 Estimation of vertical deflection based on moment–curvature analysis results.

in Eq. (14), the central deflection of the member (Δ) can be calculated numerically as shown in Fig. 14, as follows:

$$\Delta \approx \sum_{j=1}^{n} \left(\frac{\phi_j x_j + \phi_{j+1} x_{j+1}}{2} \right) \Delta x_j \tag{15}$$

Figure 15 shows the computational procedures of the nonlinear flexural analysis presented in this study. Iterative calculations have been conducted for the selected concrete strain of the extreme top fiber (ε_t) by updating the selected concrete strain of the extreme bottom fiber (ε_t) until convergence was obtained (i.e. the equilibrium condition was satisfied). The same calculations were also performed by increasing the concrete strain of the extreme bottom fiber (ε_t). In this study, it was assumed that the specimens failed in flexure when ε_t reached its ultimate value (i.e. $\varepsilon_{cu} = 0.003$).

3.2 Comparisons of Analysis Results and Test Results

Figure 16 shows a comparison between the flexural responses of test specimens and those estimated from the nonlinear flexural behavior analysis model presented in the previous section. The proposed model evaluated the cracking loads of the US-F1 and US-F2 specimens as 251.4 and 264.0 kN, respectively, which agreed well with the test results. This is because the analysis model successfully reflects the segmental effect, which is the unique characteristic of the PHWF composite girder, as shown in Fig. 17a, b. Figure 17c shows a comparison of the strain distributions at the load level of 230 kN that were estimated from the proposed analysis model with and without consideration of the segmental effect. As shown in Fig. 17a, for the case of the PSC bottom flange, which is fabricated by separate casting, the eccentricity of the strands is very small because the strands are placed around the centroid of the PSC bottom flange member. Therefore, the initial camber caused by the introduction of prestress is smaller than that of the monolithic cast section. However, since the cross-sectional area of the prestressed concrete bottom flange is small, a high level of prestress can be introduced into the concrete. Actually, the compressive stress of concrete caused by the introduction of prestress at the extreme bottom fiber of the US-F2 specimen was 8.3 MPa, but if the segmental effect was ignored (i.e. assuming monolithic casting as shown in Fig. 17b), the compressive stress reduced to 6.3 MPa. Accordingly, the cracking strength (P_{cr}) was 166.9 kN in

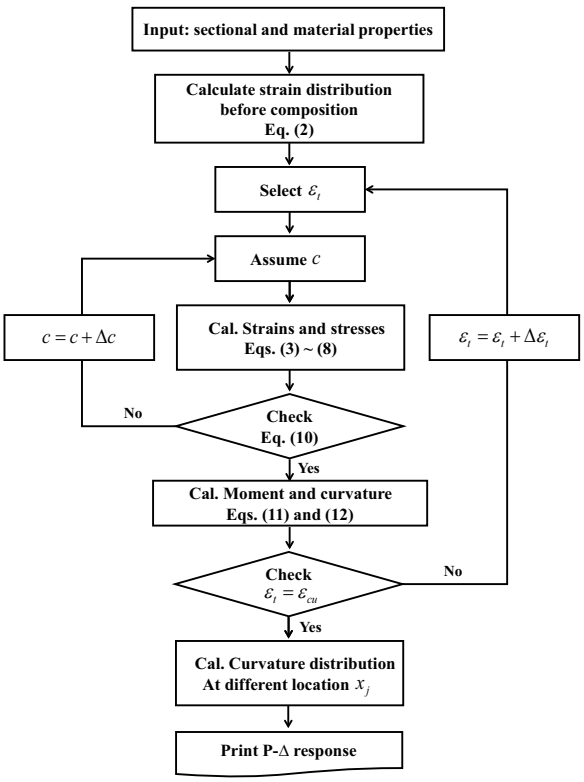

Fig. 15 Computational procedures of proposed flexural analysis model.

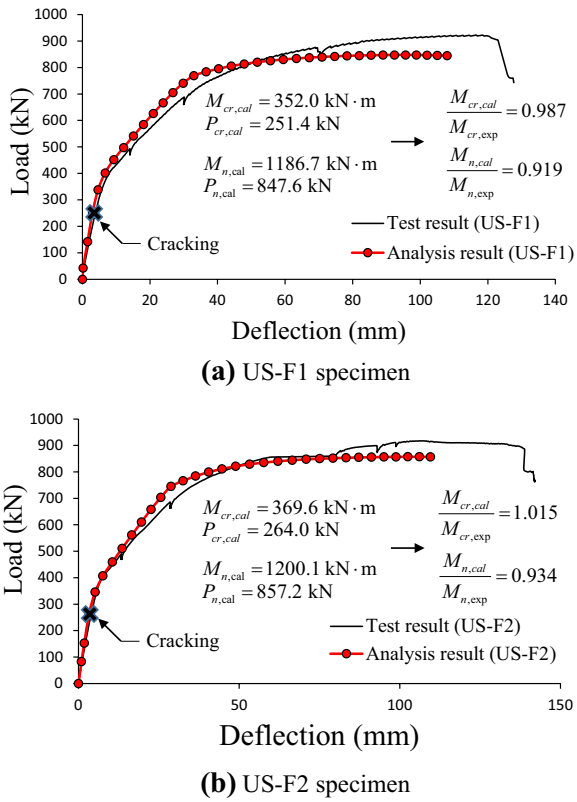

Fig. 16 Verification of proposed flexural analysis model.

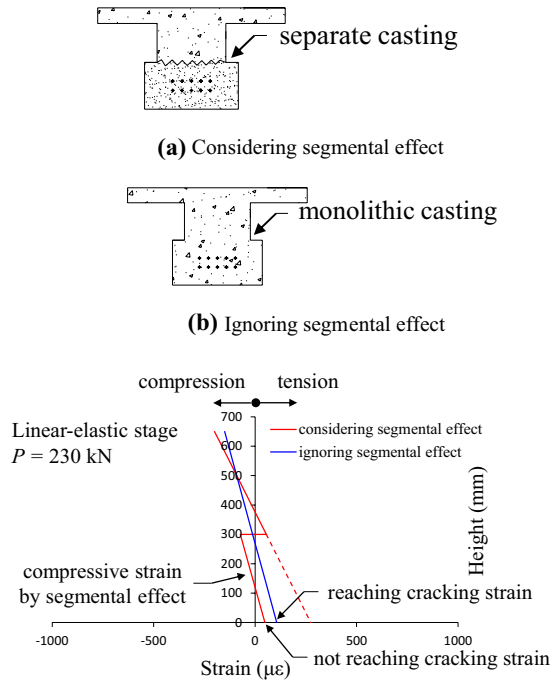

Fig. 17 Segmental effect on strain distribution of composite section.

the case of ignoring the segmental effect, but it increased to 264.0 kN when the segmental effect was considered. In addition, the proposed model estimated the flexural behaviors of the test specimens after flexural cracking with a high level of accuracy. The proposed model also estimated the maximum strengths of the US-F1 and US-F2 specimens as 847.6 and 857.2 kN, respectively, and these results are very close to the test results. Figure 18 shows comparisons between the strain distributions measured from the experiment along the section height at different loading stages and those estimated using the proposed analysis model. It was confirmed that the nonlinear flexural behavior model provides very good estimations of the strain distributions of the test specimens.

4 Conclusion

In this study, flexural tests were conducted to evaluate the flexural performances of a prestressed hybrid wide flange (PHWF) composite girder. The PHWF composite girder can efficiently resist external loads considering its unique constructional sequences. In addition, the flexural behaviors of the test specimens were analyzed in detail by utilizing the proposed nonlinear flexural analysis model. On this basis, the following conclusions were drawn:

1. The PHWF composite girder exhibited excellent flexural performances and sufficient composite performances even for the PHWF composite girder without shear connectors. It is be thus considered that the PHWF composite girder can be applied without shear connectors, which leads to a more cost-effective application.
2. The nonlinear flexural analysis model considering the segmental effect proposed in this study estimated the flexural behaviors and strengths of the test specimens with a high level of accuracy, and provided a very good estimation on the strain distributions along the section height for all loading stages.
3. Based on the detailed analysis results of the PHWF composite girders, the differences in the strain distributions and initial behaviors of the PHWF composite girders when the segmental effect is both considered and not considered, could be clearly understood.
4. However, since the embedded steel member has many trapezoidal-shaped openings in the web, analytical and experimental studies on the shear behavior of the PHWF composite girders are also required for practical application.
5. It is expected that the experimental results and nonlinear analysis model presented in this study can be utilized as fundamental information in the research fields related to prestressed steel–concrete compos-

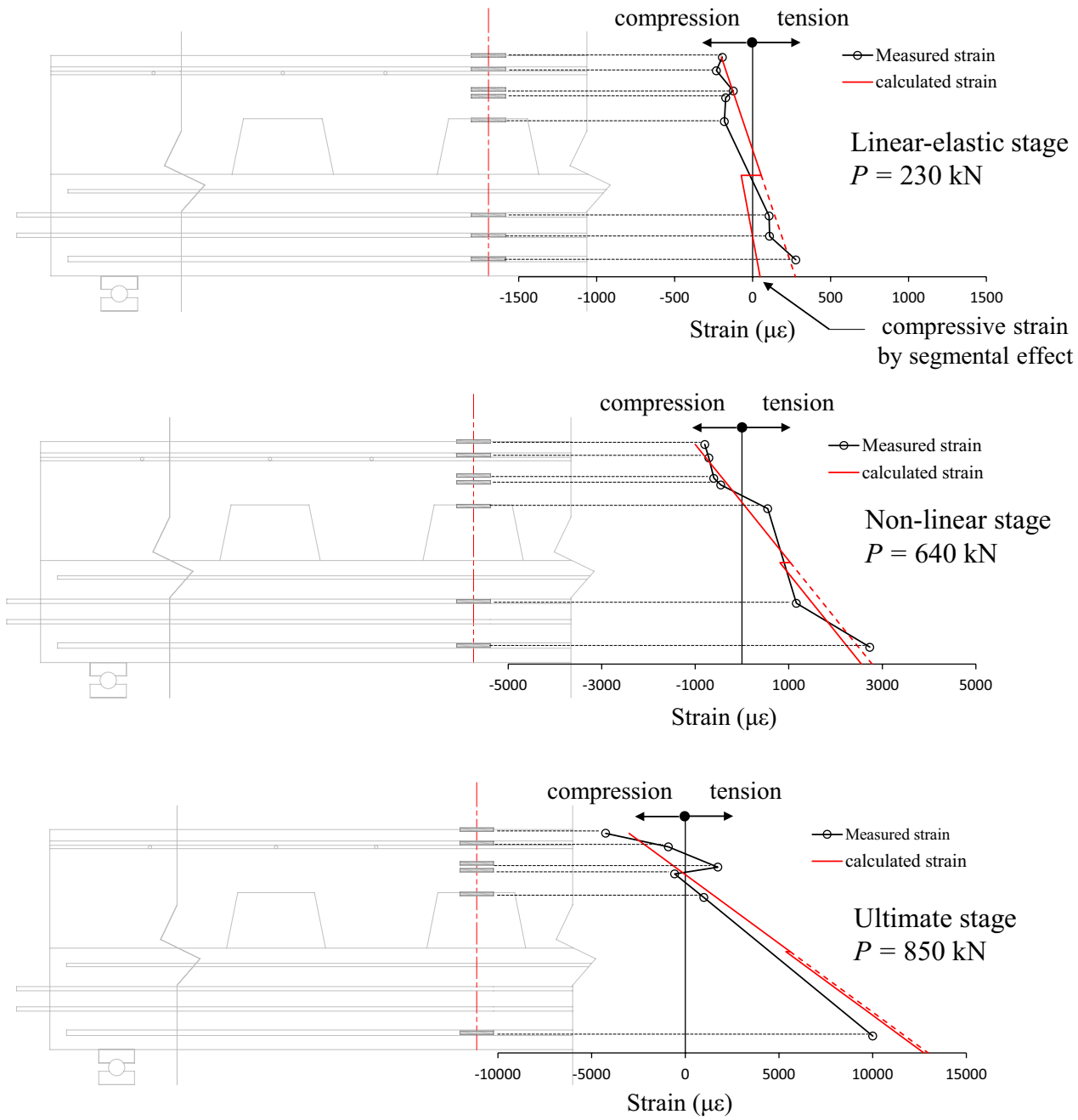

Fig. 18 Comparison of measured and calculated sectional strain distributions.

ite structures, and that this study can contribute to developing simplified design methods of segmental prestressed steel–concrete composite systems for structural engineers.

Authors' contributions

SJH wrote the original manuscript and revised the manuscript. DHL and JYO conducted experimental study, and SHC analyzed test results. KSK supervised this research and reviewed the manuscript. All authors read and approved the final manuscript.

Author details
[1] Department of Architectural Engineering, University of Seoul, 163 Siripdaero, Dongdaemun-gu, Seoul 02504, South Korea. [2] Department of Civil Engineering, Nazarbayev University, 53 Kabanbay Batyr Ave, Astana, Republic of Kazakhstan 010000. [3] Head of Research Center, Sejin R&S, 6, Eonju-ro 125-gil, Gangnam-gu, Seoul 02504, South Korea.

Acknowledgements
This research was supported by Basic Science Research Program through the National Research Foundation of Korea (NRF) funded by the Ministry of Science and ICT (2016R1A2B2010277). Authors also would like to express sincere thanks to Gilgyo Co., for supporting the fabrication of test specimens.

Publisher's Note

Received: 10 November 2017 Accepted: 28 March 2018
Published online: 02 August 2018

References

Abbas, H. H., Sause, R., & Driver, H. G. (2007). Analysis of flange transverse bending of corrugated web I-girders under in-plane loads. *Journal of Structural Engineering, ASCE, 133*(3), 347–355.

ACI Committee 318. (2014). *Building code requirements for structural concrete (ACI 318-14) and commentary*. Farmington Hills, MI: American Concrete Institute.

Ayyub, B. M., Sohn, Y. G., & Saadatmanesh, H. (1990). Prestressed composite girders under positive moment. *Journal of Structural Engineering, ASCE, 116*(11), 2931–2951.

Ayyub, B. M., Sohn, Y. G., & Saadatmanesh, H. (1992a). Prestressed composite girders. I: Experimental study for negative moment. *Journal of Structural Engineering, ASCE, 118*(10), 2743–2762.

Ayyub, B. M., Sohn, Y. G., & Saadatmanesh, H. (1992b). Prestressed composite girders. II: Analytical study for negative moment. *Journal of Structural Engineering, ASCE, 118*(10), 2763–2783.

Azizinamini, A., Barth, K., Dexter, R., & Rubeiz, C. (2004). High performance steel: Research front-historical account of research activities. *Journal of Bridge Engineering, 9*(3), 212–217.

Bae, D. B., & Lee, K. M. (2007). Behavior of preflex beam in manufacturing process. *KSCE Journal of Civil Engineering, 8*(1), 111–115.

Collins, M. P., & Mitchell, D. (1991). *Prestressed concrete structure*. Englewood Cliffs: Prentice Hill.

Heo, B. Y. W., Kwak, M. K., Bae, K. W., & Heong, S. W. (2007). Flexural capacity of profiled steel composite beams: deep deck plate. *Journal of Korean Society of Steel Construction, 19*(3), 247–258.

Hong, W. K., Kim, J. M., Park, S. C., Kim, S. I., Lee, S. G., Lee, H. C., et al. (2010a). Composite beam composed of steel and precast concrete (Modularized Hybrid System, MHS). Part II: Analytical Investigation. *Structural Design of Tall and Special Buildings, 18*(8), 891–905.

Hong, W. K., Park, S. C., Kim, J. M., Lee, S. G., Kim, S. I., Yoon, K. J., et al. (2010b). Composite beam composed of steel and precast concrete (Modularized Hybrid System, MHS). Part I: Experimental investigation. *Structural Design of Tall and Special Buildings, 19*(3), 275–289.

Hong, W. K., Park, S. C., Kim, J. M., Lee, S. G., Kim, S. I., Yoon, K. J., et al. (2010c). Composite beam composed of steel and precast concrete (Modularized Hybrid System, MHS). Part IV: Application for multi-residential housing. *Structural Design of Tall and Special Buildings, 19*(7), 707–727.

Hong, W. K., Park, S. C., Lee, H. C., Kim, J. M., Kim, S. I., Lee, S. G., et al. (2010d). Composite beam composed of steel and precast concrete (Modularized Hybrid System, MHS). Part III: Application for a 19 story building. *Structural Design of Tall and Special Buildings, 19*(6), 679–706.

Kim, J. H., Kim, D. K., Lee, J. H., & Kim, J. H. (2009). Static behavior of concrete-filled and tied steel tubular arch (CFTA) Girder. *Journal of Korean Society of Steel Construction, 13*(3), 225–231.

Kim, S. B., Kim, S. S., & Ryu, D. S. (2013). Study on the cyclic seismic testing of U-shape hybrid composite beam-to-composite column connections. *Journal of Korean Society of Steel Construction, 25*(1), 47–59.

Kim, K. S., & Lee, D. H. (2011). Flexural behavior of prestressed composite beams with corrugated web: Part II. Experiment and verification. *Composites Part B Engineering, 42*(1), 1617–1629.

Kim, K. S., Lee, D. H., Choi, S. M., Choi, Y. H., & Jung, S. H. (2011). Flexural behavior of prestressed composite beams with corrugated web: Part I. Development and analysis. *Composites Part B Engineering, 42*(1), 1603–1616.

Kim, J. H., Park, K. H., Hwang, Y. K., Choi, Y. M., & Cho, H. N. (2002). Experimental study for the development of steel-confined concrete girder. *Journal of Korean Society of Steel Construction, 14*(5), 593–602.

Lee, D. H., Oh, J. Y., Kang, H., Kim, K. S., Kim, H. J., & Kim, H. Y. (2015). Structural performance of prestressed composite girders with corrugated steel plate webs. *Journal of Constructional Steel Research, 104*(1), 9–21.

Oh, J. Y., Lee, D. H., Cho, S. H., Kang, H., Cho, H. C., & Kim K. S. (2015). Flexural behavior of prestressed steel-concrete composite members with discontinuous webs. *Advances in Materials Science and Engineering*, Article ID: 278293, 1–13

Oh, J. Y., Lee, D. H., & Kim, K. S. (2012). Accordion effect of prestressed steel beams with corrugated webs. *Thin-Walled Structures, 57*(1), 49–61.